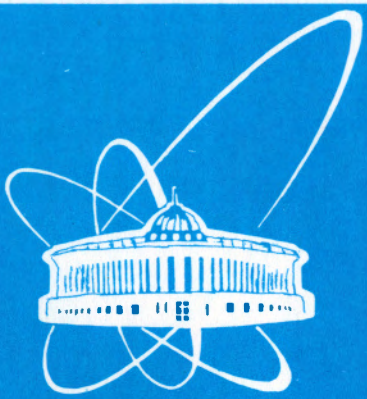

СООБЩЕНИЯ
ОБЪЕДИНЕННОГО
ИНСТИТУТА
ЯДЕРНЫХ
ИССЛЕДОВАНИЙ

Дубна

E7-99-239

WIDE APERTURE MULTIPOLE MAGNETS OF THE KINEMATIC SEPARATOR **COMBAS**

Analyzing Multipole Magnets M1 and M8 with Compensation for Higher Order Aberrations

1999

Артюх А.Г. и др.
E7-99-239

Широкоапертурные мультипольные магниты кинематического сепаратора КОМБАС.
Анализирующие мультипольные магниты M1 и M8
с компенсацией аберраций высоких порядков

Создан и введен в эксплуатацию высокоразрешающий широкоапертурный кинематический сепаратор КОМБАС, магнитная структура которого выполнена на принципе жесткой фокусировки. В состав сепаратора входят восемь широкоапертурных мультипольных магнитов M1—M8. Первый и последний магниты, M1 и M8, содержат в распределении поля мощные квадрупольные и октупольные компоненты. Наличие данных компонентов позволило отказаться от квадрупольных линз, а также добиться минимизации сферических аберраций и компенсации хроматических эффектов. Для магнитов M1 и M8 проведены трехкомпонентные магнитные измерения, позволившие определить качество их изготовления, а также составить трехмерные карты магнитного поля. Карты полей магнитов предполагается использовать для проведения траекторных расчетов по трассировке частиц через сепаратор.

Работа выполнена в Лаборатории ядерных реакций им. Г.Н.Флерова ОИЯИ.

Сообщение Объединенного института ядерных исследований. Дубна, 1999

Artukh A.G. et al.
E7-99-239

Wide Aperture Multipole Magnets of the Kinematic Separator COMBAS.
Analyzing Multipole Magnets M1 and M8 with Compensation
for Higher Order Aberrations

The high-resolving large aperture kinematic separator COMBAS has been created and commissioned. The magneto-optical structure of separator is based on the strong focusing principle. The separator consists of eight wide aperture multipole magnets M1—M8. The first and the last magnets, M1 and M8, contain power quadrupole and octupole components in their field distributions. The presence of these components allowed one to intensify focusing without quadrupoles, minimize spherical aberrations and compensate for chromatic effects. Three-component magnetic measurements of the multipole magnets M1 and M8 have been performed. These measurements let both compile 3D-maps of the magnetic fields and analyze the magnet manufacturing quality. The 3D-maps of the magnetic field are supposed to be used for the particle trajectory simulations along the separator.

The investigation has been performed at the Flerov Laboratory of Nuclear Reactions, JINR.

Communication of the Joint Institute for Nuclear Research. Dubna, 1999

A.G.Artukh, G.F.Gridnev, Yu.G.Teterev
Joint Institute for Nuclear Research, 141980, Dubna, Russia

M.Grushezki, F.Koscielniak, J.Szmider
Henryk Niewodniczanski Institute for Nuclear Physics, Crakow, Poland

A.G.Semchenkov*, O.V.Semchenkova, Y.M.Sereda, I.N.Vishnevski
Institute for Nuclear Research, Kiev, Ukraine

V.A.Shchepunov
Laboratorio Nazionale del Sud INFN, 95123 Catania, Italy

Yu.P.Severgin, V.L.Vasiljev, Yu.A.Myasnikov, B.V.Rozhdestvenski, A.Yu.Konstantinov, V.V.Koreniuk, E.A.Lamzin, M.G.Nagaenko, S.E.Sytchevski
Efremov Scientific Research Institute of Electrophysical Apparatus, St. Petersburg, Russia

*E-mail: semchenkov@main1.jinr.ru

1. Introduction

Analyzing magnets are an essential part of a separating system based on the separation only with magnetic field. When the COMBAS separator was being under design, a decision was taken not to use electric fields, as great values of voltage are required to separate particles having magnetic rigidity as large as 4.5 T*m. Apart from this, to achieve larger angular acceptance both in the vertical and horizontal planes a separator must be the strong focusing one. The use of focusing quadrupoles in the magnetic structure of a separator confines, however, itself the device aperture, because of the intrinsic aperture limits, which quadrupole magnets have due to the saturation phenomenon. Therefore, the focusing functions, usually performed by quadrupoles, were transferred to wide-aperture magnets having non-uniform magnetic fields [1-3]. On this basis analyzing magnets M1 (12KH55 ESN162.5-1.125-25) (Fig.1) and M8 have been designed and produced (Fig. 2).

One should note that the multipole magnet M1 together with multipole magnet M2 make up the analyzing section of the separator [1-3] and, in the linear approximation, completely determine the system's optical properties. Magnet M1 focuses in the vertical plane and defocuses in the horizontal plane. The action of magnet M2 on the beam is reverse. The 1st order field indexes of M1 and M2 are opposite in sign. The use of such a magnetic structure let, flexibly and efficiently, form a beam of required profile and size and, in addition, to facilitate the minimization for the higher order spherical aberrations, which increase considerably the image size in wide-aperture systems.

2. Basic performance data of the magnets

The principles embodied in the design of magnets M1, M8 are outlined in [1-3]. The magnets M1, M8 (Fig.2) have the 1st order field index n=11.0024, the bending radius and deflection angle 4m and 25 deg respectively. The gap between pole pieces of the magnets is varying, the greater values of the gap correspond to the greater bending radii. The pole pieces are of a special form to produce quadrupole and octupole field components. The basic performance data of the magnets are given in table 1.

A real challenge was the manufacturing of the magnets. The main problem was to make pole pieces of the required shape. The four magnet poles were produced from a single piece of an iron blank. A special merry-go-round machine, whose rotatable section's diameter was as large as 10m, has been used. This let produce pole pieces having identical shape and magnetic properties.

3. Measuring magnetic characteristics

3.1. Magnetic measurements

The distributions of the M1 and M8 magnetic field induction have been measured twice. The first measurements were performed at the manufacturing works in Saint Petersburg, where the magnetic curves and fields' distributions in the median plane for two levels of the magnetic flux density, $\mathbf{B_0}$=2770Gs and $\mathbf{B_0}$=8800Gs, were obtained and analyzed. Then three-component magnetic measurements were carried out (Fig. 3) in the FLNR JINR (Dubna).

In the measurements in Saint Petersburg the cartesian coordinate system **(OX,OY(ΔR),OZ)** have been used with the origin (0, 0, 0) lying at the center of the

magnet, the axis **OX** tangential to the magnet optical axis at its center and pointed in the direction of motion of the beam, the radial axis **OY(ΔR)** laying in the magnet central section, directed towards the greater bending radius and the vertical axis **OZ** directed down. The measuring system was manually operated and consisted of a bar holding the Hall probes and a set of the graduated guides. The reference of the measuring system to the magnet was performed with the help of a theodolite. The system was set in such a way that the Hall probes were always in the magnet median plane (with the accuracy of 0.1 mm). The positioning accuracy along the **OX** and **OY** axes was estimated to be not worse than 0.2 mm. The magnetic field measuring accuracy was not worse than 2 Gauss, i.e. not more than 0.02% of the magnetic field value at the magnet center. To reduce measurement errors, each value was measured five times.

The r.m.s. error of the field measurements due to both the head positioning errors and the errors of the Hall probes voltage readout was not higher than 3 Gauss, i.e. not more than 0.04% of the field in the magnet center. Such an error reasonably met the set requirements on the magnetic field forming.

To carry out three-component measurement of the magnets M1 and M8, the automated measuring system (Fig. 3) has been created at FLNR JINR. The system included the following components (Fig. 4):

- two heads for measuring three components $\mathbf{B_x}$, $\mathbf{B_y}$ and $\mathbf{B_z}$ of the magnetic field. Each head included three Hall probes (having dimensions 2*2*0.1 mm) located at distances 10 mm from each other along the axis **OX**. The probe positioning accuracy within the measuring head was 0.1 mm. A special bench has been used to calibrate the angle of rotation of the probes around the axes **OZ**, **OY** and **OX** (this was not more than 2 degrees). The field components reciprocal dependences were taken into account in the final build of the magnetic field map;

- two monitoring probes for monitoring the temperature and time stability during the prolonged magnetic measurements. The probes were placed in a narrow part of the gap with a high magnetic field of more than 10 kGs. The probes' readouts have been used to normalize the results of the magnetic measurements;
- a measuring carriage equipped with two separable plates, enabling the heads to be installed, was produced with the accuracy of 0.1 mm;
- guides, which enabled moving the measuring carriage inside the magnets;
- an electrical drive including steppers (two step motors SHD-5) and a belt of stainless steel moving the measuring carriage along the guides with an accuracy of 0.02 mm (step of SHD-5) along the **X**- and **Y**-axes;
- assemblies for controlling the supply of the steppers, the controlling subassembly installed in the IBM PC;
- a channel for measuring the current of the Hall probes built on the basis of the SOLARTON precision digital voltmeter (voltage measuring accuracy being 1 mkV) having a digital exit and the SOLARTRON 7010 MINATE commutator;
- a computer control program for controlling the steppers, the eight-channel system for the readout of the measured data from the digital voltmeter and writing the data on the IBM PC hard disc according to the standard RS-232.

The Hall probes were first calibrated, using a special magnet having a uniform field, with the help of the NMR magnetometer (having accuracy of 0.001%). At each point measurements were performed 5 times. The r.m.s. error of measuring the magnetic field due to magnetic heads positioning errors (caused by the magnetometer assembly errors and the positioning accuracy with the steppers) and errors of measuring the voltage was not more than 2 Gauss, or 0.03% of the field in the center of the magnet. The measurements were taken using the cartesian coordinate system having

- the **OX**-axis tangential to the magnet radius at the magnet central point;
- the **OY**-axis directed towards the greater radius at the magnet central point;

- the **OZ**-axis, vertical, directed down according to the positive value of the induction.

Along the **X**- and **Y**-axis in the measuring plane, the assemblies of the heads were moved automatically with the step of 20 mm, while along the **Z**-axis, the assemblies were hand-operated (with 10 mm step). The measurements have been performed in 15 planes. The magnetic field was measured in the range of ± 1280 mm along the **X**-axis, +200/-420 along the **Y**-axis and ± 70 mm along the **Z**-axis (from the magnet center) for three field levels in the center: $\mathbf{B_0}$=7050 Gs (current 550 amps.), $\mathbf{B_0}$=9440 Gs (current 700 amps.) and $\mathbf{B_0}$=11610 Gs (current 900 amps.). The total number of the measured points in each plane was more than 4000.

3.2. The magnetization curve

The measured magnetization curve (circles) is shown in the fig.5 in comparison with simulated points. The measurements were performed in the center of the magnet M1. The experimental magnetization curve has stronger induction growth as compared with the simulated points. For example, this difference at the point **I**=700amps. is 500 Gs (7.9%).

3.3. Analysis of the field distribution in the central section

The induction distributions of the magnets M1 and M8 were analyzed with the procedure described in [3]. The measurements displayed that the difference between induction values in M1 and M8 did not exceed 0.2%. In other words, the magnets M1 and M8 are practically identical.

The magnetic field distribution in the central section of M1 is shown in the Fig.6 for the field level B_0=7050Gs. As one can see quadrupole and octupole components are presented in the distribution. Namely, the quadrupole component shows itself as a linear decrease of the field from smaller to larger radii. (Respectively, the gap enlarges from smaller to larger radii.) The octupole component contribution is seen in a slight deviation of the curve behavior from the linear low at minimum and maximum radii typical for 3rd order polynomials.

Analysis of the measurement data, obtained in Dubna, displayed that the deviation of the measured values from the calculated ones was, within the working area of the magnets of ± 200 mm, not more than 0.1% for the field level B_0=7050Gs. For levels B_0=9440Gs and B_0=11610Gs such deviations do not exceed 0.2% and 0.5% respectively. In the wider range of ± 350 mm the values of deviations did not exceed 1% for the all field levels. The measured points lie very close to the calculated curves so as the deviations are within the design limits [2]. This is the result of good quality magnet manufacturing. Some increase of errors in the minimum gap (or higher field) region at smaller radii is as large as 0.5% that is probably due to the saturation effects. This can decrease slightly the working width of the magnet up to ± 150 mm (75% of the nominal width) for magnetic rigidities above 4.0 T*m.

Analysis of the fields measured in Saint Petersburg showed that the deviations of the measured values from those calculated are less than 0.1% for B_0=2770 Gs and B_0=8800 Gs.

3.4. Analysis of the field distribution in the median plane

The procedure of the analysis of the median plane field has been described in [3]. The measurements have been done in the rectangular coordinate system with the origin placed in the center of the magnet.

Fig.7 presents the measured B_z-component of the magnetic field in the median plane of M1 for the field level B_0=7050 Gs (the B_x- and B_y-components in the median plane are equal to zero). The field distribution along the **OY**-axis at **X**=0 corresponds to that presented in the Fig.6. The positive value of B_z corresponds to the direction downwards. Analysis of the measurement data obtained in Dubna showed that the effective length errors are less than 1.0%, 0.7% and 1.5% from the design value for the field levels B_0 equal to 7050, 9440 and 11610 Gauss, respectively. The measurements made in Saint Petersburg discovered these errors to be less than 1.5% and 0.9% for the field levels B_0 equal to 2770 and 8800 Gauss, respectively. The pole face rotation error in the fringing field areas is as large as 2.5, 1.5, 1.2, 1.0 and 0.5 degrees for the B_0 equals, respectively, to 2770, 7050, 8800, 9440 and 11610 Gauss.

3.5. The magnetic field distributions in the plane 30mm below the median one

One of the main purposes of the tree-component magnetic field measurements performed in Dubna was that of obtaining **3D** magnetic field maps of the all magnets, in part M1 and M8, to be used subsequently for the computerized particle raytracing through the entire separator. For this we have measured the B_x-, B_y- and B_z-components of the magnetic fields in 15 planes: in the median plane and in the planes parallel to and situated below and above the median one in the range ± 70 mm spaced with the step 10 mm.

Fig. 8 and 9 represent respectively the measured B_x and B_y component of the field of the magnet M1 in the plane situated 30 mm below the median plane for the field level B_0=7050 Gauss. The component B_x is the projection of the magnetic field vector on the unit vector tangential to the M1 optical axis and located in the center of

the magnet. The component $\mathbf{B_y}$ is the projection of **B** on the direction along the bending radius pointing towards the larger radii.

The evolution of $\mathbf{B_x}$ along the axis **OX,** typical for any dipole magnet, can be understood easily from Fig.10 a) showing schematically the **XOZ** section of M1. As the coordinate **X** changes from big negative to big positive values passing through the magnet the component $\mathbf{B_x}$ subsequently grows, reaches its maximum positive value in the vicinity of the effective field boundary, decreases and passes zero value in the center of the magnet, and then repeats the same evolution but in the opposite order and with the opposite sign. One can see from Fig.8 that the absolute values of the $\mathbf{B_x}$ maximums (minimums) near the entrance (exit) EFB's are bigger at smaller **Y**. This is due to smaller gap sizes and, hence, higher magnetic flux densities in the area of smaller **Y**.

The behavior of the component $\mathbf{B_y}$ is rather complicated. However, as one can see from Fig.9 it has obvious mirror symmetry with respect to the plane **YOZ** passing through the center of the magnet.

Fig.11 presents the measured distribution of the component $\mathbf{B_z}$ in the plane situated 30 mm below the median plane for the field level $\mathbf{B_0}$=7050 Gauss. The character of the distribution in the central section repeats that for the median plane (see Fig.6). As compared with the behavior of $\mathbf{B_z}$ in the median plane (see Fig.7), the values of $\mathbf{B_z}$ in this distribution drop faster from its maximum values to zero when the effective field boundaries are crossed.

4. Conclusion

The magnetic measurements of M1 and M8 displayed good manufacturing quality. In particular, the all field distributions have good symmetry, which is a result of the good quality magnet assembling and the absence in the pole pieces of shells and domains having higher magnetization. The measurements also showed a complete identity of the magnet pair M1, M8. The differences in the induction values in the median plane are not greater than 0.2%, and in the effective magnetic lengths 0.05%.

The magnetic field errors in the central section of the magnets do not exceed 0.5% at the maximum value of the field. These errors decrease and do not exceed the design limits at the nominal and less than nominal values of the magnetic flux densities. The errors of the effective lengths and fringe fields are maximal at minimum values of the magnetic induction and as large as 1.5% and 2.5 deg respectively. At nominal magnetic flux densities 5000-10000Gs the main magnetic parameters are within the tolerances set at the separator design stage.

The main result of the magnetic field measurements and analysis is the fact that the magnets M1 and M8 satisfy the design parameters in the range of magnetic rigidities from 2 to 4 T*m. This range is the main working one. Within this range the field and effective length errors do not exceed 0.2% and 1.0% respectively. The error pole face rotations in the fringing field areas, not exceeding 1.2 deg.

The performed tree-component magnetic field measurements allowed one to compose the 3D maps for the three field levels. This data will be used for the particle raytracing throughout the separator.

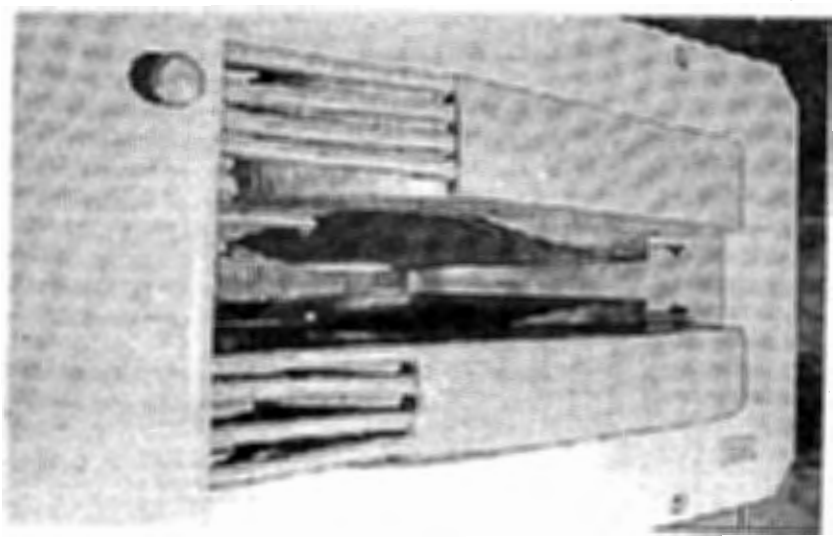

Fig.1. Analyzing multipole magnet M1 (12KH55 ESN162.5-1.125-25).

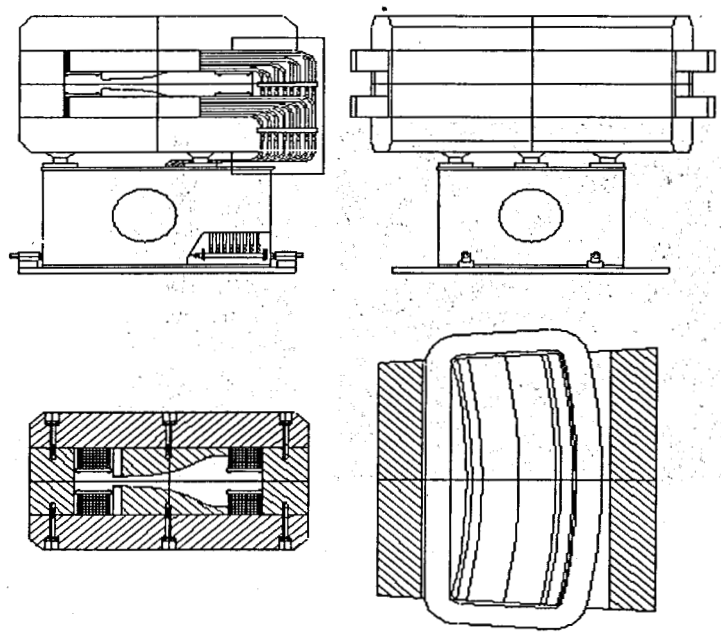

Fig.2. The drawings and sections of multipole magnets M1, M8.

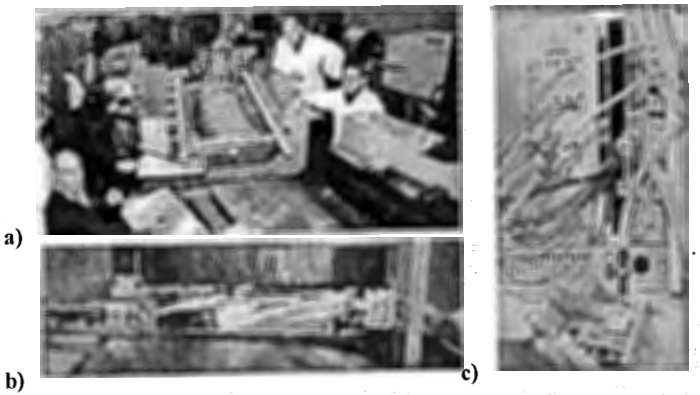

Fig.3. Measuring the magnetic characteristics of the magnet M1 in Dubna (FLNR JINR).

a) Mounting the measuring system on the magnet M1.

b) The magnet M1 measuring system mounted in the magnet gap.

c) The measuring head having three aligned (**OX**-axis) Hall probes positioned at the angle of 90 degrees to each other.

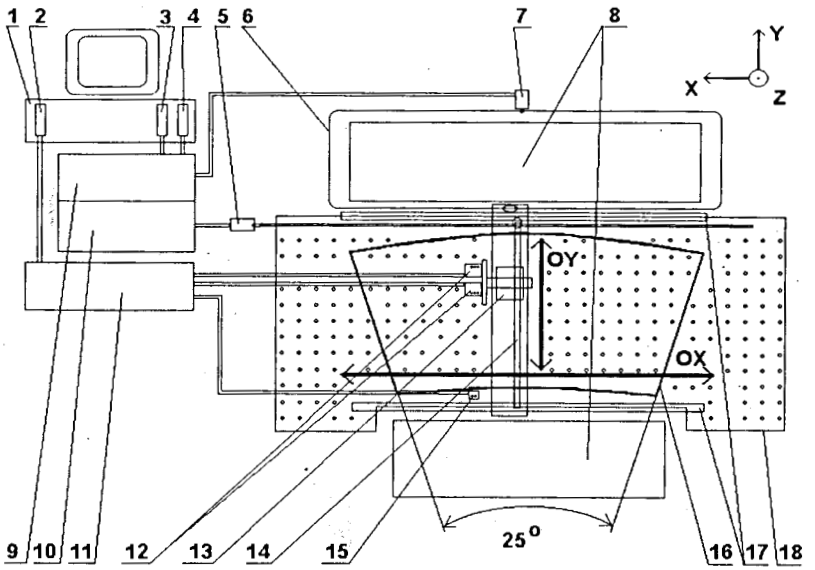

Fig.4. Block diagram of the automated system for measuring the magnetic field of the magnets M1 and M8. Figure denote:

1- the control computer IBM PC AT (486);
2- the controller for connection with the SOLARTRON digital voltmeter;
3- the controller for the power supply assemblies of the **X**-coordinate displacement stepper;
4- the controller for the power supply assemblies of the **Y**-coordinate displacement stepper;
5- the **Y**-coordinate displacement stepper;
6- the **X**-coordinate displacement belt drive;
7- the **X**-coordinate displacement stepper;
8- the magnet M1;
9- the power supply module for the **X**-coordinate displacement stepper;
10- the power supply module for the **Y**-coordinate displacement stepper;
11- the SOLARTRON precision digital voltmeter;
12- two measuring heads, each having 3 Hall probe;
13- the measuring carriage;
14- the **Y**-coordinate displacement belt drive;
15- the monitoring Hall probes;
16- the area within effective field boundaries(deflection angle 25 deg, radius $\mathbf{R_o}$=4m);
17- the measuring carriage guides;
18- the magnetic field measurement area.

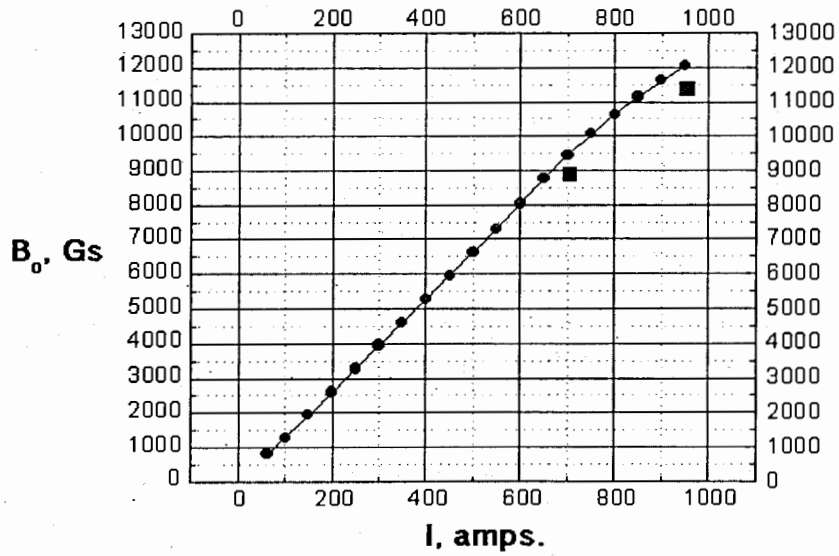

Fig.5. The magnetization curve of the magnet M1. The squares – theoretical calculations, the circles – experimental points.

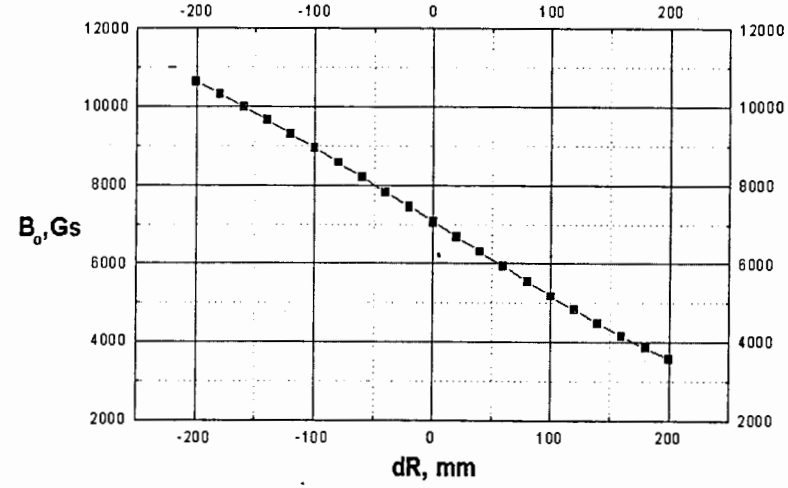

Fig.6. The magnetic field distribution in the central section for the field level B_0=7050Gs. The measured points coincide with the values, calculated according to the equations (3) and (4) [3], with the accuracy better than 0.1%.

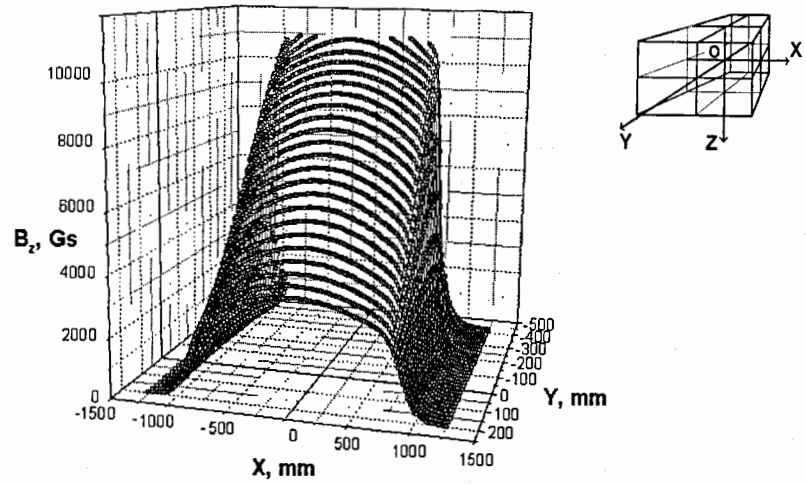

Fig.7. The measured distribution of the B_z-component of the magnetic field in the median plane.

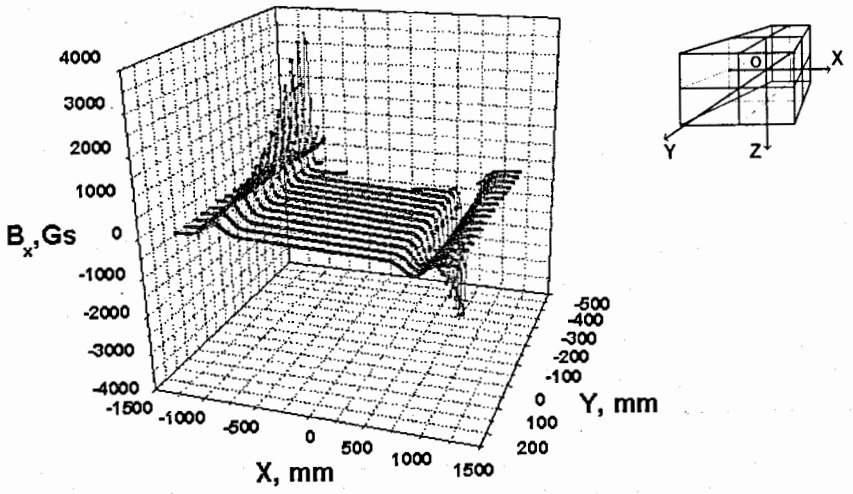

Fig.8. The measured distribution of the $\mathbf{B_x}$-component of the magnetic field in the plane 30mm below the median plane.

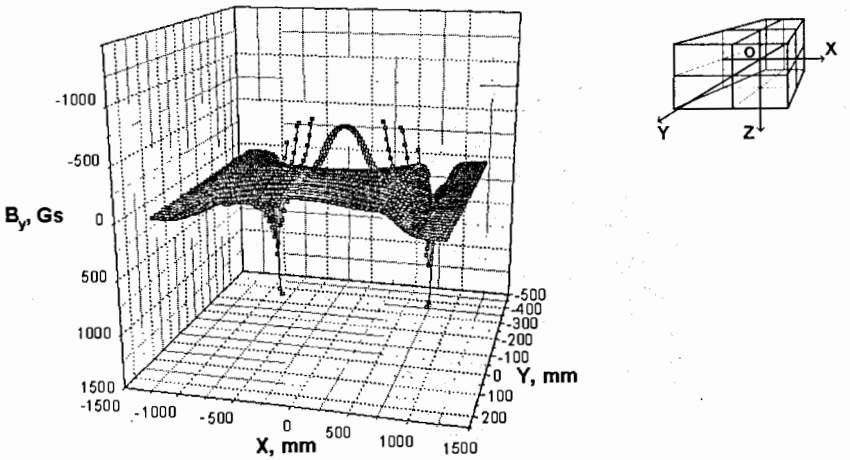

Fig.9. The measured distribution of the $\mathbf{B_y}$-component of the magnetic field in the plane 30mm below the median plane.

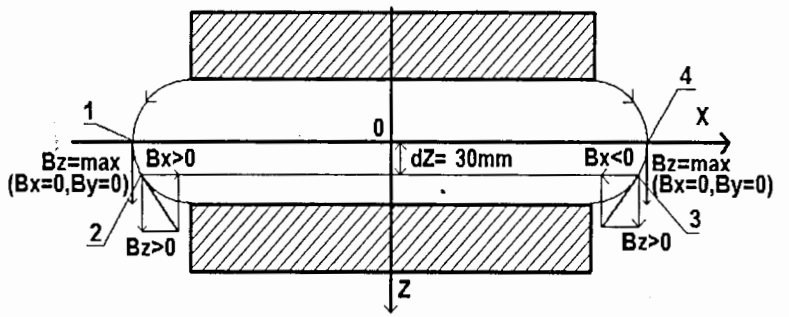

a)

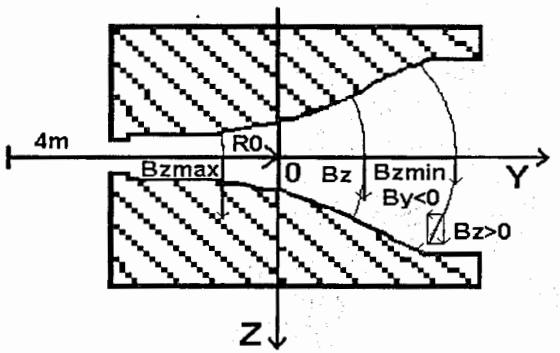

b)

Fig.10. The sketchy image of the vertical sections of the magnet M1 in the measurement planes **XOZ** (a) and **YOZ** (b). The axes **OX** in the figure a) and **OY** in b) lie in the median plane. Field lines going from the upper to the lower pole are shown. The directions of the magnetic field vector are indicated with arrows in the points 1-4, points 1,4 belonging to the median plane and 2, 3 to the plane situated 30 mm below the median one.

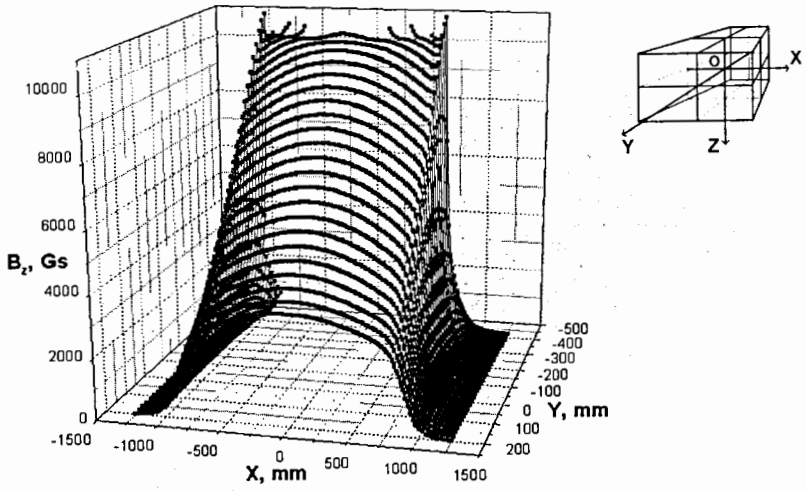

Fig.11. The measured distribution of the B_z-component of the magnetic field in the plane 30mm below the median plane.

Table 1.

The basic parameters of the magnets M1(M8).

Parameters	Values
Maximum induction on the central trajectory (T)	1.125
Nominal induction on the central trajectory (T)	0.875
Radius of the central trajectory (m)	4
Working width of the pole pieces (mm)	400(± 200)
Gap along the central trajrctory (mm)	120
Effective length (mm)	1746
Deflection angle (deg)	25
Resistance of coils (Ω)	0.07
Maximum current (amp.)	950
Rated current (amp.)	700
Maximum Voltage (v)	70
Rated Voltage (v)	50
Maximum Power (kwatt)	66.5
Rated Power (kwatt)	35
Inductance of coils (H)	0.17
Water discharge (liter per minute)	23
Water overheading (C)	40
Copper mass (tns)	1.1
Steel mass (tns)	13.3
Total magnet mass (tns)	15

5. Acknowledgments

The authors are indebted to Yu.Ts.Oganesian and V.Z.Majdikov for the fruitful discussions and support. We appreciate A.A.Alexeeva for the preparation of manuscript.

6. References

1. A.G.Artukh et al., Nucl. Instr. and Meth. A 306 (1991) 123.
2. A.G.Artukh et al., Nucl. Instr. and Meth. A 426 (1999) 605.
3. A.G.Artukh et al., Magnets of The Wide Aperture Separator COMBAS. Basic Principles of Magnet Design, Commun. JINR E7-99-238, Dubna, 1999.

Received by Publishing Department
on September 9, 1999.